Transient Magnetic Analysis of Voltage Pulse excited Induction Machines with respect to Diagnosis and Fault Detection

M.A. Samonig and Th.M. Wolbank
Vienna University of Technology,
Department of Energy Systems and Electrical Drives
Gußhausstraße 25-29/370-2, 1040 Vienna, Austria
Tel.: +43 (1) 58801 - 370226
E-Mail: thomas.wolbank@tuwien.ac.at
URL: http://esea.tuwien.ac.at/

ACKNOWLEDGEMENTS

The work to this investigation was supported by the Austrian Science Fund (FWF) under grant number P23496-N24.

ABSTRACT

A new fault detection method for induction machines (IM) is analyzed with respect to transient magnetic material behavior by means of finite element (FE) modeling. The detection method uses the machines inverter to excite the IM with transient voltage pulses and measures the corresponding phase current responses. To account for the material behavior transient BH curves are identified from measurements on a demagnetized magnetic circuit and included in the FE model to accurately simulate pulsed voltage excitations.

KEYWORDS

«Simulation», «Induction motor», «Converter machine interactions»

INTRODUCTION

The majority of proposed fault detection methods so far is limited to mains fed operation and uses current signature analysis (CSA) to identify fault indicators, namely sidebands in the stator current [1]. CSA and methods closely related to it are working well for mains fed machines with changing load levels, yet they are limited to quasi-steady state conditions of stator frequency and load in terms of inverter operation. An essential requirement of many methods to detect a broken rotor bar is a minimum load level of 30-40%, to guarantee a detectable interaction of the fault with the fundamental wave. A detection method for zero load is presented in [2] by measuring the rotor time constant in different spatial directions. Other works [3]-[6] propose injection of rotating or pulsating signals into the machine at standstill, [6] requires a loaded machine, though.

The new fault monitoring technique for inverter-fed IM proposed in [7] is applicable at zero speed. In addition it requires no load, as the inverter is used to excite the machine's phases with a sequence of voltage pulses. This pulses cause transient current responses in the machine phases that hold information on saliencies and asymmetries within the machine, which can clearly be exploited to extract a fault indicator.

One common feature of most methods is the detection of variations in the machine stator inductance, which are characteristic for machine asymmetries. To analyze this effect various FE simulations have been implemented [8]-[10]. A common conclusion is that faults cause redistributing flux paths, e.g. flux perturbations in the vicinity of a damaged rotor bar. Investigations done in [8] and [9] give a vivid analysis of this effect for saturable machines and fundamental wave excitation. In [10] simulations of broken rotor bars during mains-fed operation are carried out. Amongst other results the slip (load) dependency of straightforward CSA is shown, which is caused by varying extension of flux perturbations. For high slip values the perturbations concentrate around the broken bar, whereas low slip causes an extension over the entire air gap making it increasingly difficult to distinguish the fault

signal and fundamental wave. This results in the well known masking effect as the left/right side component and the fundamental frequency merge to an increasing degree.
A possible way to overcome this problem, especially for inverter-fed machines, is the introduction of an excitation signal that is of "high frequency" compared to the fundamental wave. In [4] this is done with a pulsating voltage space vector up to some 100 Hz. The method proposed in [7] uses a sequence composed of some 10µs long inverter pulses, according to some 10 kHz. To analyze this fault detection method in terms of flux distribution and adaptability to different machine designs a transient FE model was used and compared to measurement results in [11]. In this case the magnetic properties were modeled with a linear material approximation. The results for winding currents and their time derivatives, which are used to extract the fault indicator, were in good agreement with measurements on a test machine and the model basically is capable of showing the influence of machine asymmetries on the flux distribution. Due to the used linear material model the simulated flux distribution was assumed to be a rough approximation of the "real" one, especially for transient (high frequency) excitations. Thus, the present paper is aimed at refining the FE model with a more sophisticated magnetic model, derived from transient magnetic measurements on a stator core composed of the same material as the IM. Similar research has been executed in [12] but aimed at implementation with a magnetic equivalent circuit.
As the investigated detection method is based on the measurement of current responses due to high frequency voltage excitations, the material model's influence on the current change is of special interest. The next chapter is aimed at giving the reader a short introduction to the derivation of the mentioned fault indicator, which forms the starting point for further investigations.

PRINCIPLES OF ANALYZED FAULT DETECTION METHOD

The key aspects of the fault detection method under investigation shall be summarized in the following chapter. A more detailed explanation can be found in [7].

As already mentioned above, a common feature of many fault detection approaches is the identification of stator inductance variations. A distinctive feature of the considered detection method is the derivation of a robust fault indicator by utilization of the drives internal sensors only (i.e. the inverters current sensors) to non-invasively measure the value of phase current. If the used inverter is of voltage source type the maximum terminal voltage resembles the DC link. The relationship between the two input quantities is given by the stator equation (1).

$$\underline{v}_S = r_S \cdot \underline{i}_S + l_l \cdot \frac{d\underline{i}_S}{d\tau} + \frac{d\underline{\lambda}_R}{d\tau} \tag{1}$$

As shown by this equation the stator voltage phasor $\underline{v}_S$ is an addition of the voltage drop impressed by the stator current phasor $\underline{i}_S$ on the stator resistance r_S, the voltage related to the change of the stator current $d\underline{i}_S/d\tau$ in the leakage inductance l_l and the time derivative of the rotor flux $\underline{\lambda}_R$ (back EMF).
With help of the DC link the machine's phases can be excited with pulses by simply switching between maximum DC link voltage and short circuit state at the IM terminals. Due to high frequency conditions the leakage inductance effective differs from that for the fundamental wave. To account for this behavior a transient leakage inductance $l_{l,t}$ is introduced in the stator equation (1), which leads to (2) and (3). Indices *I* and *II* are used for positive and negative pulse excitations, respectively. The reason for the use of voltage pulses of both polarities will become clearer when equation (5) is derived later on.

$$\underline{v}_{S,I} = r_S \cdot \underline{i}_{S,I} + l_{l,t} \cdot \frac{d\underline{i}_{S,I}}{d\tau} + \frac{d\underline{\lambda}_{R,I}}{d\tau} \tag{2}$$

$$\underline{v}_{S,II} = r_S \cdot \underline{i}_{S,II} + l_{l,t} \cdot \frac{d\underline{i}_{S,II}}{d\tau} + \frac{d\underline{\lambda}_{R,II}}{d\tau} \tag{3}$$

A machine without saliencies would be characterized by a scalar transient leakage inductance $l_{l,t}$. But this case does usually not occur, not even for a perfectly symmetrical IM. There are always saliencies imposed by the machine geometry (e.g. rotor/stator slotting) and even more important by machine faults (e.g. broken rotor bars or eccentricities). As these saliencies cause a variation of the machine's

effective air gap length, they also influence the transient leakage inductance and consequently are observable in the resulting current change.
In terms of the space phasor representation used in the equations this is taken into account by introduction of a complex transient leakage inductance $\underline{l}_{l,t}$, (4). This complex quantity comprises two parts: the constant l_{const} and a modulation with the amplitude l_{mod}, which varies with the spatial position γ of the maximum inductance within one pole pair, also shown in Fig. 1.

$$\underline{l}_{l,t} = l_{const} + l_{\mathrm{mod}} \cdot e^{j2\gamma} \tag{4}$$

During the next step the above mentioned voltage pulses of inverse polarity, represented by (2) and (3) are subtracted from each other. This is done to eliminate the resistive voltage drop and the back EMF. The result is shown in (5).

$$\underline{v}_{S,I} - \underline{v}_{S,II} = \underline{l}_{l,t}\left(\frac{d\underline{i}_{S,I}}{d\tau} - \frac{d\underline{i}_{S,II}}{d\tau}\right) = \underline{l}_{l,t}\left(\frac{d\underline{i}_{S,I-II}}{d\tau}\right) = \underline{v}_{S,I-II} \tag{5}$$

For an IM at standstill without fundamental wave excitation ($\underline{i}_S$=0, $\underline{\lambda}_S$=0) equation (5) is perfectly valid. Elimination of these two components is also valid for rotating, energized machines as long as the stator current phasor and back EMF between positive and negative voltage pulse only show negligible changes. Mathematically this is expressed by the following statements:

$$\underline{i}_{S,I} \approx \underline{i}_{S,II}, \qquad \frac{d\lambda_{R,I}}{d\tau} \approx \frac{d\lambda_{R,II}}{d\tau} \qquad \text{and} \qquad \frac{d\underline{i}_S}{d\tau} \approx \frac{\Delta \underline{i}_S}{\Delta\tau}. \tag{6}$$

In addition the time derivative of the current is approximated by the difference Δ in (6). Finally inversion of (5) yields (7).

$$\frac{\Delta \underline{i}_{S,I-II}}{\Delta\tau} = y_{const} \cdot \underline{v}_{S,I-II} + \underline{y}_{\mathrm{mod}} \cdot \underline{v}_{S,I-II} = \underline{y} \cdot \underline{v}_{S,I-II}. \tag{7}$$

Like the complex leakage inductance the reactance variable $\underline{y}$ is complex valued and consists of a constant and a spatial position dependent part. Therefore it includes information on all machine saliencies and permits the extraction of a fault indicator. A graphical two pole representation of this relationship for a pulse in direction of machine phase L1 (real axis α) is shown in Fig. 1. In this picture the movement of the current change phasor $\Delta\underline{i}_{S,I-II}/\Delta\tau$ defines the dashed circle and is characteristic for a certain saliency, i.e. circle diameter and movement relative to one mechanical rotor revolution. For a broken bar for example, the phasor tip rotates with twice the angular frequency of the fundamental wave (periodicity factor n = 2) because the bar causes the same inductance variation when passing the two poles of one pole pair during its rotation, regardless of their polarity. In case of the saliency caused by Qr rotor slots this inductance variation frequency is of dγ/dt times Qr ($n = Qr$), but shows a lower diameter.

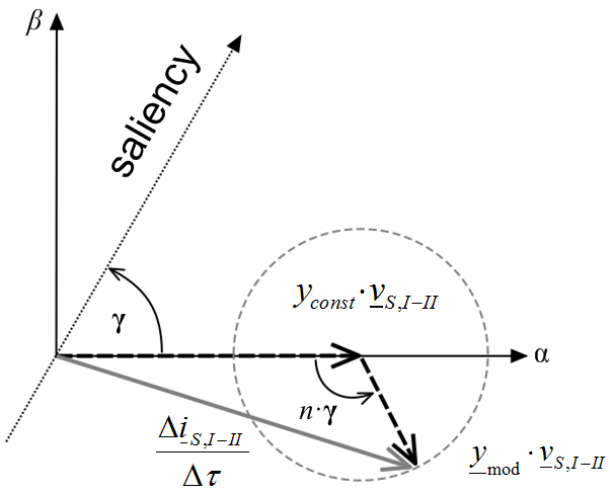

Fig. 1. Current slope trajectory for an applied voltage phasor $\underline{v}_S$ in direction of phase L1 (axis α) for a given saliency, charaterized by a certain diameter and periodicity n, relative to the spatial position γ.

In this way all saliencies are represented by a periodic circulating current change phasor resulting in a superimposed saliency indicator. Thus, the indicator for a given fault induced saliency can be extracted by spatial Fourier analysis.

PULSED EXCITATION OF MAGNETIC CIRCUIT

The IM's laminated stator/rotor core is composed of stacked ferromagnetic steel sheets. In order to get deeper insight into the transient magnetic material behavior and consecutively to derive a suitable material model for transient FE simulations an empirical approach was chosen. This means measurements on a stator core equipped with excitation and measurement windings around its yoke - from now on referred to as "Magnetic Circuit" (MC) - were carried out, as shown in the following paragraph.

Magnetic Circuit Measurements

The specimen used to identify the transient ferromagnetic material behavior was a standard IM stator core, composed of sheets (M800-50A), without a three-phase winding in its slots. Instead an excitation winding around its yoke was introduced to form a closed magnetic circuit.

As the analysis in this paper concentrates on investigations of an IM at standstill without fundamental wave excitation, measurements were made for demagnetized material. Demagnetization was achieved by applying a varying magnetic field to the specimen and stepwise reduction of its amplitude to zero. This was done with the voltage source inverter (VSI) usually used to supply the IM. After this procedure the VSI was also used to apply voltage pulses of different magnitude (5V, 12.5V, 25V, 50V, 100V, 150V and 220V) but equal duration (30µs) to the specimen. The current response representing the MC magnetizing current was measured with an oscilloscope. In order to eliminate the influence of winding resistance and leakage inductance a measurement winding was introduced to measure the induced voltage. From these values the field intensity at the mean ring diameter and the mean flux density were derived and gave the materials BH curve for the given excitation. After that, each curve was approximated by a fitting function to eliminate measurement noise and guarantee a smooth permeability profile. Curves calculated this way are shown in Fig. 2 along parts of initial and stationary magnetization curves. Results in Fig. 2 show the impact of varying excitation magnitude on transient material behavior. One obvious conclusion is that each excitation level corresponds to a different BH curve. Based on this observation the paper aims at deriving a more accurate material modeling procedure for transient FE simulations of a demagnetized voltage driven specimen in the next chapter.

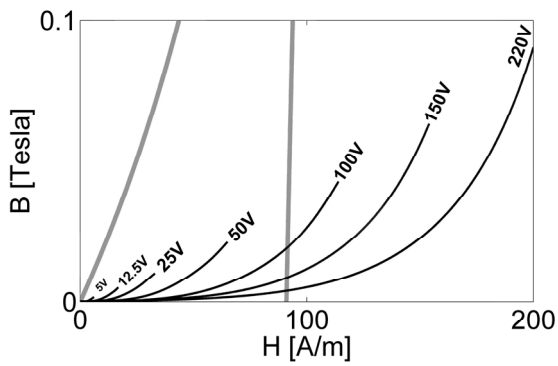

Fig. 2: BH-curves for 30µs pulse excitations (black) with varying voltage magnitude (5V–220V) in comparison to initial and stationary magnetization curve (grey) for demagnetized specimen.

Magnetic Circuit Simulation

When simulating transient excitations of the MC with a voltage pulse of certain magnitude, the first thought is to model the magnetic material by using the corresponding transient BH curves. For a 220V pulse this would mean that the MC core is modeled with "homogeneous" material properties by assigning the nonlinear transient 220V BH curve of Fig. 2 to all finite elements in the area. Left part of Fig. 3 shows the results of such a simulation. Although the simulated current response is in good

agreement with the measured one, it is questionable if this also applies to the calculated flux distribution, shown in the lower part of Fig. 3. The main problem is observable in this figure, though. It can be traced back to the inhomogeneous distribution of excitation levels within the MC core. In other words the outer parts of the MC experience a lower rate of flux change than the inner parts, which is equivalent to a lower excitation voltage. Consequently the approximation of the whole magnetic material by just one BH-curve is not correct.
A possible way to overcome the mentioned problem is the introduction of excitation dependent BH-curves, like the ones shown in Fig. 2. Seven of these transient curves were identified by measurements. However, a greater number is desirable in order to achieve better discretization and simulation results. Therefore a total of 300 different curves were interpolated and extrapolated respectively, corresponding to excitation levels from 1V to 300V.

As usual the transient FE simulation is split up into time steps of certain duration. Within each step a nonlinear solution is calculated before moving on to the next one. In the proposed simulation process additional material allocation iterations are introduced before the next time step is started. This process comprises the following steps.

1) For the first iteration a "homogeneous" material distribution is used to get an initial approximation of the flux density within the MC. To speed up the subsequent material iteration processes it is desirable to use one of the transient BH curves displayed above. The flux density end values for all finite elements obtained from this first iteration are stored and the next iteration is initiated.
2) From the stored flux density values of the previous step and the known pulse duration (30µs) the associated local rate of flux change is calculated for each element. Each rate of change corresponds to one of the transient magnetization curves, which is then assigned to the examined finite element for the next iteration. After this process the simulation of the given time step is restarted with the new material distribution. The difference from the initial "homogeneous" iteration is that the material representation is "inhomogeneous" now. At the end of this step the flux density values are stored again for the next iteration.
3) These iterations are repeated as long as a self defined convergence criterion is not complied with. Basically this criterion monitors the current change between subsequent iterations and waits for the moment when the current is oscillating between two values, indicating that the material assignment process switches between adjacent values for each element too.

Results of the described simulation procedure can be found in the right part of Fig. 3.

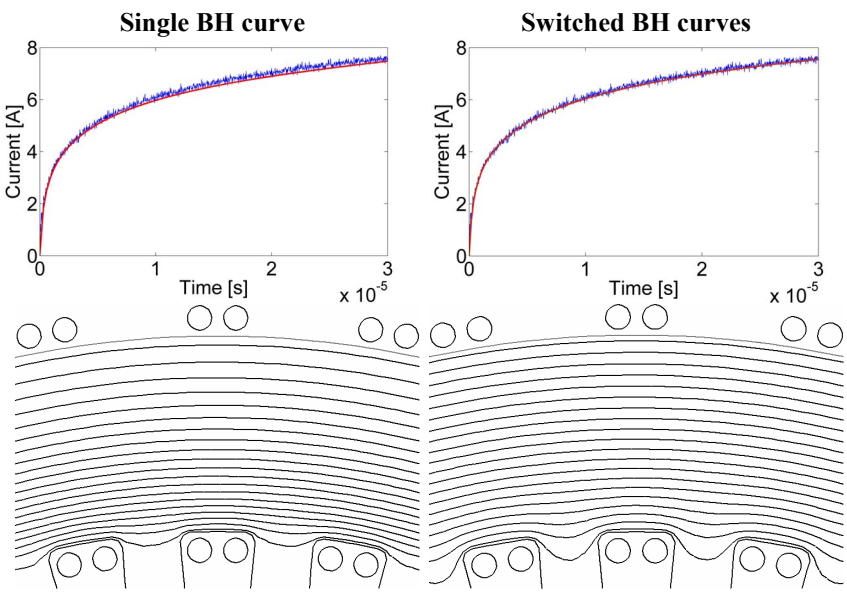

Fig. 3: ***Top***: Measured (blue) current responses and results of nonlinear (red) simulations for excitation of demagnetized magnetic circuit with a 220V, 30µs pulse. ***Bottom***: Flux density plots for 220V transient excitation, for the different modeling approaches: single BH curve (left) and switched BH curves (right).

The comparison of simulated and measured current response proves the quality of the new material model, as the deviations are negligible. In addition it illustrates the differences between the flux distribution for the single BH and the newly proposed model, from now on labeled “switched BH”. What can be observed is a more accurate simulation of the flux distribution in the MC's outer parts and a deeper penetration into the tooth areas caused by transient dynamic material processes.

PULSED EXCITATION OF INDUCTION MACHINE

Starting from the considerations in the previous chapters the mentioned fault detection method will be analyzed in the following sections. This is done by comparing simulation results for different linear and nonlinear material representations to measurements. The nonlinear simulations give results for single and switched BH curves. Investigations begin with the analysis of a faultless IM in the next paragraph and after that move on to a faulty case with a fully broken rotor bar. Due to the similarities between MC and IM (basically the squirrel cage IM is just a magnetic circuit with an air gap and an additional short-circuited winding) the switched BH simulation procedure does not need adaptation and can be adopted exactly as presented above.

Faultless Induction Machine Simulation

This section is intended to verify the correct implementation of the proposed material model. Therefore simulation results for a faultless IM are presented and compared to measurements to check their plausibility.

In Fig. 4 plots for measured and simulated current responses are shown. One obvious difference from similar plots of the MC (Fig. 3) is an increased linearity in their course. This linearization effect originates from two sources. First, the magnetic circuit of an IM is not solely composed of electrical steel as the test MC above. It also comprises an air gap between stator and rotor that increases the needed magnetomotive force (MMF) for a given magnetization level and therefore causes one part of the observed shearing effect. The second and more dominant share in this effect has the squirrel cage, which presents a barrier for instant flux changes and thus expulses the flux into the air gap. This effect is depicted in the left part of Fig. 5 and increases the air gap influence for transient excitations, which leads to the dominant shearing effect exposed in Fig. 4.

Another prominent part is a transient oscillation process at the beginning of the measured current course. These oscillations originate from the difference of machine and line impedance. This causes a reflection of the excitation voltage pulse at the machine terminals, which consequently leads to transient overshoot of voltage and current values. The simulated current courses in Fig. 4 don’t show these oscillations, as a 2D FE model was used and the supply line was not considered. At first sight all results, regardless of the used material model, seem to give good approximations of the real conditions. The model using single 220V BH curve is the one delivering the least coincidence with the measurement.

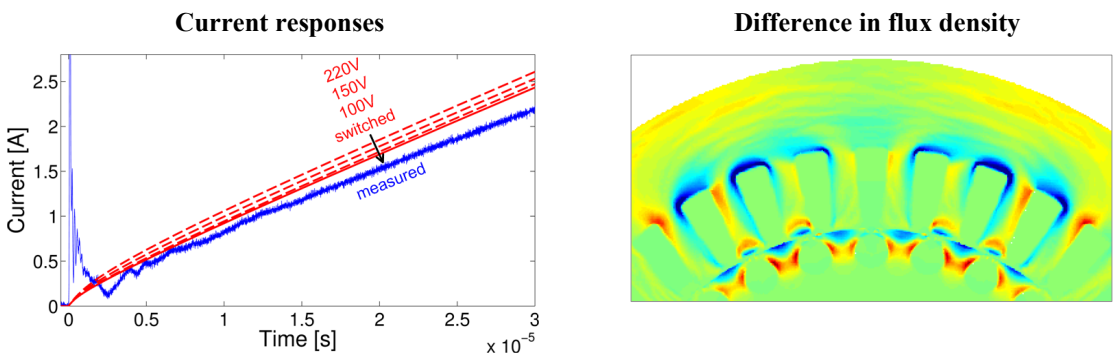

Fig. 4: ***Left*** picture: Measured (***blue***) current response and results of nonlinear simulations (***red***) for excitation of demagnetized IM with a 440V, 30µs pulse. Dashed courses show (from top to bottom) results for: 220V, 150V and 100V single BH curve. Solid course shows switched BH model results. ***Right*** picture: Difference in flux density distribution between single 100V and switched BH model. Warm colors (***red***) indicate an increase, cold colors (***blue***) a decrease.

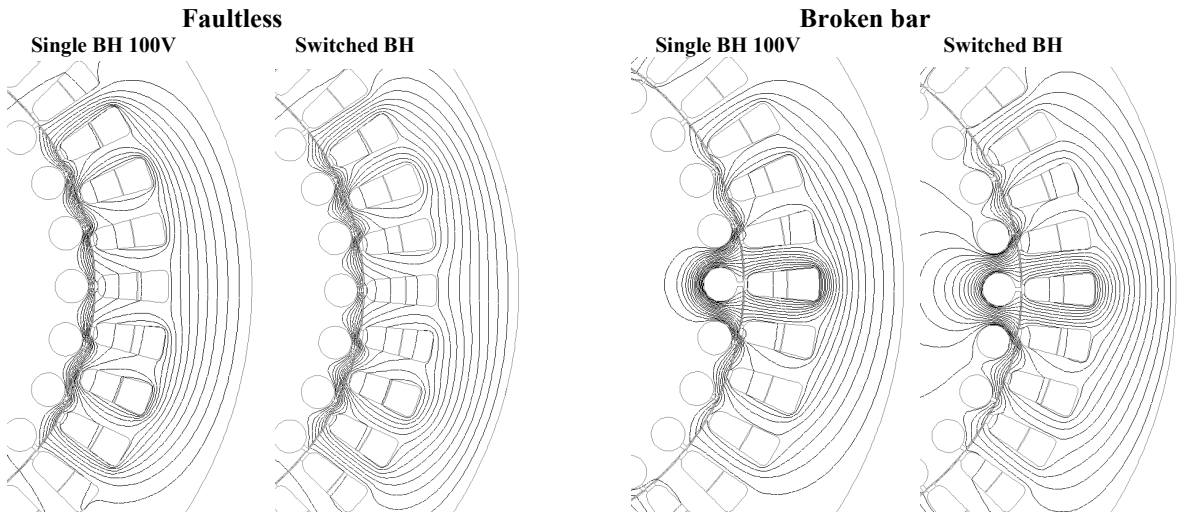

Fig. 5: Flux line plot for pulse excitation of an IM in faultless condition (***left***) and with a broken bar (***right***) for single and switched BH models.

The switched BH model along with 100V BH curve gives the most accurate results. It is not surprising that the 100V single curve delivers results comparable to the switched model ones, because the corresponding level of excitation lies somewhere in the middle of all monitored excitations in the IM body. Therefore it can be interpreted as an average material representation, which delivers good results for simulated current courses. However, if flux density distributions of single and switched BH model are compared to each other a considerable deviation can be observed in the right part of Fig. 4. It shows the flux density difference for single and switched BH model at 30µs, which corresponds to an increase in wide tooth and yoke regions of about 100 percent. As the observed change is quite dominant its influence on the fault indicator is analyzed in the next chapter. Fig. 5 shows the same effect but due to the chosen representation as flux line plot it is not as clearly visible in case of the faultless IM.

Although the simulation gives decent results an additional deviation from measurements is observable. The reason for this can probably be found in the used 2D model representation, which does not account for 3-dimensional effects that alter the machine leakage inductance, i.e. end windings and rings of stator and rotor, respectively. If the mentioned 3D effects were known for the given excitation conditions, the neglected machine parts could be modeled by an additional constant leakage inductance. The problem herein lies in the identification of these inductance values. Especially for pulsed excitations their determination is difficult, as empirical formulas usually are only given for harmonic considerations. Nevertheless it was tried to approximate the end winding leakage inductance value with such well known formulas. From calculations in the frequency range of some 10 kHz corresponding to the excitation duration a value of some hundred µH was identified. Simulations with an additional serial inductance of this magnitude resulted in better results. Further investigations will have to be made though, in order to verify the switched BH model in this respect, ideally with a 3D FE model to get a better approximation of the end winding inductance.
Furthermore, a comparison of simulation and measurement results for test machines with same geometry but different stator windings (2, 4 and 6 poles) showed an improvement in simulation accuracy with increasing pole number. To explain this effect the corresponding end winding leakage inductances were estimated, which revealed decreasing tendencies with pole number, whereas the remaining parts of leakage inductance (given by machine data sheets) increased for the investigated test machines. In other words the end winding leakage inductance has a bigger share in overall leakage inductance for the two pole machine as for higher pole numbers. Consequently neglecting this inductance value in the 2D model has bigger influence for the two pole machine, which can explain the reduced agreement with measurement results.

Because of its nature as a constant factor the neglected leakage share is of minor importance for the comparison of linear, single and switched BH models with respect to the fault indicator in the next chapter.

Broken Rotor Bar Simulation

As already mentioned in the chapter "Principles of Analyzed Fault Detection Method" the breaking of a bar in a squirrel cage IM introduces a fault induced saliency to the machine. Although in this case the word asymmetry is better used, as the fault disturbs the machine symmetry (here: squirrel cage symmetry). This can be observed in Fig. 5, where the broken bar gives the flux a possibility to bypass the rotor slot by deeper penetrating the rotor core. The consequence is an increased leakage inductance, which in turn reduces the measured current slope of Fig. 6 compared to the faultless case. Therefore the period of the introduced asymmetry corresponds to the number of poles that the bar is passing during one mechanical revolution. This leads to a harmonic in the spatial leakage inductance spectrum of the same order (n = 2 for two poles) with respect to one mechanical revolution (γ=360°), which means 2 cycles of the saliency trajectory in Fig. 1. During one of these cycles the current change phasor passes the points of minimum and maximum length, thus defining the trajectory diameter. These two points correspond to the two rotor positions γ=0° (minimum) and γ=360°/2n (maximum). The diameter is of special interest as it is used to derive the fault (asymmetry) indicator. In order to give a clear statement about whether the use of a more complex material model improves simulation results for faulty conditions or not, it is important to determine the influence of the various material models on this indicator. This is done by comparing the current slope values at the mentioned rotor positions.

Fig. 6 shows measured and simulated results for minimal and maximal current change phasor. It has to be noted that the 100V BH curve was used in case of the single BH material model, because it showed the highest coincidence with the switched BH approach in the faultless case. In case of the faulty IM the deviations in current courses again are negligible. With respect to the flux distribution the same effect as observed in the faultless case shows deeper yoke and tooth penetration in wide regions with differences of up to 100% between single and switched material model, though.

Another effect that can be seen in Fig. 6 is that the deviation from measurements is lower for the simulated minimum current slopes (lower traces in the diagram) than for the maximum ones (upper traces). The deeper flux penetration into the rotor (see Fig. 5) causes an increase in transient leakage inductance, whereas the end-winding leakage remains unchanged. As a result, the influence of the end winding portion is reduced. For the maximum current rotor fault position the transient leakage inductance passes its minimum and the influence of end winding leakage inductance becomes more dominant, which results in a bigger difference between simulation and measurement. These results follow the same pattern as observed for different pole numbers in the previous chapter and thus consolidate the assumption that unconsidered 3D effects are responsible for the simulation inaccuracies.

Finally a comparison of linear, single and switched models has been carried out to quantify the impact of different material models on simulation results for the current slope change (difference between min. and max. current slope values), from which the fault indicator is derived.

Current responses **Difference in flux density**

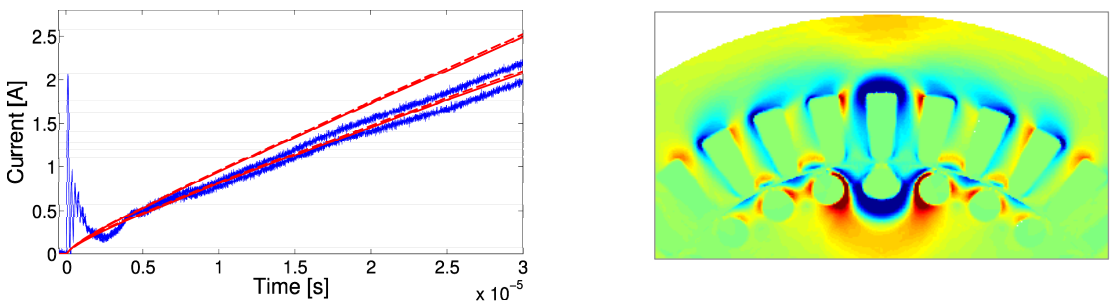

Fig. 6: ***Left*** picture: Maximum (upper) and minimum (lower) courses of measured (***blue***) and simulated (***red***) current responses for 440V, 30µs pulse excitation of an IM with one broken rotor bar. Dashed courses show results for the 100V single BH curve. Solid courses illustrate switched model results. ***Right*** picture: Difference in flux density distribution between single 100V and switched BH model. Warm colors (***red***) indicate an increase, cold colors (***blue***) a decrease.

TABLE I lists a comparison of this difference for each of the tested modeling approaches and compares them to measurements. It can be seen that the deviation from measurement results for linear model approaches lies in the range of 50-60%. This deviation range of 10% depends on whether a constant permeability value is chosen that resembles the end value of differential permeabilities ($\mu_r \sim 1000$) in the curves of Fig. 2, or an absolute permeability value ($\mu_r \sim 360$), defining a linear increase from zero to maximum flux densitiy in Fig. 2. The nonlinear models show similar deviations of about 53%. With respect to current slope simulation an accuracy gain for the switched model could not be detected, despite the previously shown differences in flux distribution.

TABLE I: Comparison of current change rates

	$(\Delta I_{max} - \Delta I_{min})/\Delta t$ [A/ms]	Difference from measurement
Linear curves (μ_r = 360, 500, 750, 1000 and 1400)	13.91-14.71	50-60%
Single curves (100, 150 and 220V)	~14.10	~53%
Switched curves	14.11	~53%
Measurement (Reference value)	9.229	-

Conclusion

A new modeling and simulation approach for demagnetized voltage driven magnetic circuits under pulsed excitation has been derived and implemented in a FE model to analyze its influence on simulation accuracy of current responses due to high frequency pulse excitations with respect to diagnosis and fault detection. Since the investigated fault detection method is based on the derivation of a fault indicator from the variation in current change rates, the models influence on these rates was of special interest. In this respect results for the new model showed only negligible differences compared to “simpler” approaches. However some conclusions for the FE modeling of pulse excited voltage driven IM can be drawn.

1) A linear model delivers good approximation of the current response, especially when an absolute permeability (derived from measurements) is used. The main drawback however lies in the practical estimation of this averaged value.
2) If single nonlinear BH curves are used that also include the dynamic material behavior, simulation accuracy for current slope analysis virtually stays the same. The reason for this can be found in the IM’s air gap and squirrel cage that in combination cause a dominant linearization effect, which in turn reduces the impact of the high initial current change rates observed in case of the MC. Furthermore, this included dynamic material behavior shows minor influence on the current courses after 10 µs, but can become important if an investigation focuses on these first 10µs after the switching instant.
3) Although the proposed switched BH model does not show improvements in simulation accuracy for current slope analysis it delivers more realistic results if absolute current values are of interest. In this context it aids in identifying a suitable “averaged” material approximation, representing the average of all excitation levels in the ferromagnetic material.
4) Results showed the switched BH model’s considerable influence on the simulated flux distribution, illustrating increased flux penetration into tooth and yoke regions due to dynamic magnetic effects. Therefore the switched BH approach shows significant advantages if the transient operation of these regions is investigated.

In addition to the mentioned conclusions, results suggest further investigations on the influence of 3D effects not modeled by the used 2D approach. In order to verify the made assumptions concerning the end winding leakage inductance future research regarding the calculation of this neglected machine parts are encouraged.

References

[1] A. Bellini, F. Filippetti, C. Tassoni and G. Capolino.: “Advances in Diagnostic Techniques for Induction Machines,” IEEE Trans. Industrial Electronics, vol.55, no.12, pp.4109-4126, 2008

[2] T. Wolbank, J. Machl, R. Schneiderbauer.: “Detecting Rotor Faults in Inverter-Fed Induction Machines at Zero Load,” Proc. International Power Electronics and Motion Control Conference, EPE-PEMC, Riga, Latvia, pp.1-6, 2004

[3] S. B. Lee, J. Yang, J. Hong, B. Kim, J. Yoo, K. Lee, J. Yun, M. Kim, K. Lee, E. J. Wiedenbrug, and S. Nandi.: “A New Strategy for Condition Monitoring of Adjustable Speed Induction Machine Drive Systems,” Proc. IEEE International Symposium on Diagnostics for Electric Machines, Power Electronics and Drives, SDEMPED, pp.1-9, 2009

[4] B. Kim, K. Lee, J. Yang, S. B. Lee, E. Wiedenbrug and M. Shah.: “Automated detection of rotor faults for inverter-fed induction machines under standstill conditions,” IEEE Energy Conversion Congress and Exposition, pp.2277-2284, 2009

[5] C. Concari, G. Franceschini and C. Tassoni.: “Self-commissioning procedures to detect parameters in healthy and faulty induction drives,” Proc. IEEE International Symposium on Diagnostics for Electric Machines, Power Electronics and Drives, SDEMPED, pp.1-6, 2009

[6] B. Akin, A. B. Ozturk, H. A. Toliyat and M. Rayner.: “DSP-Based Sensorless Electric Motor Fault-Diagnosis Tools for Electric and Hybrid Electric Vehicle Powertrain Applications,” IEEE Trans. Vehicular Technology, vol.58, no.6, 2679-2688, 2009

[7] Th.M. Wolbank, P. Nussbaumer, H. Chen and P.E. Macheiner.: “Monitoring of Rotor Bar Defects in Inverter-Fed Induction Machines at Zero Load and Speed,” IEEE Trans. Industrial Electronics, in print 2011

[8] J. Sprooten, J.-C. Maun.: “Influence of Saturation Level on the Effect of Broken Bars in Induction Motors Using Fundamental Electromagnetic Laws and Finite Element Simulations,” IEEE Transactions on Energy Conversion, pp.557-564, 2009

[9] G.Y. Sizov, A. Sayed-Ahmed, C.-C. Yeh, N.A.O. Demerdash.: “Analysis and Diagnostics of Adjacent and Nonadjacent Broken-Rotor-Bar Faults in Squirrel-Cage Induction Machines,” IEEE Transactions on Industrial Electronics, pp.4627-4641, 2009

[10] J.F. Watson, D.G. Dorell.: “The Use of Finite Element Methods to Improve Techniques for the Early Detection of Faults in 3-phase Induction Motors,” IEEE Transactions on Energy Conversion, pp.655-660, 1999

[11] M.A. Samonig, P. Nussbaumer, G. Stojicic, Th.M. Wolbank.: „Analysis of rotor fault detection in inverter fed induction machines at no load by means of finite element method,” IECON - 37th Annual Conference on IEEE Industrial Electronics Society, pp.1758-1763, 2011

[12] T.M. Wolbank, R. Wöhrnschimmel, H. Hauser.: „Transient Simulation of Lamination Material Properties in Electrical Machines,” IEEE Transactions on Industrial Electronics, pp.607-612, 2002